ISSN 0021-3640, JETP Letters, 2019, Vol. 109, No. 9, pp. 559–563. © Pleiades Publishing, Inc., 2019.
Russian Text © The Author(s), 2019, published in Pis'ma v Zhurnal Eksperimental'noi i Teoreticheskoi Fiziki, 2019, Vol. 109, No. 9, pp. 579–583.

ASTROPHYSICS AND COSMOLOGY

Mass Composition of Cosmic Rays with Energies above 10^{17} eV According to the Data from the Muon Detectors of the Yakutsk EAS Array

A. V. Glushkov[a], * and A. V. Saburov[a], **

[a] *Shafer Institute of Cosmophysical Research and Aeronomy, Yakut Research Center, Siberian Branch, Russian Academy of Sciences, Yakutsk, 677891 Russia*

**e-mail: glushkov@ikfia.ysn.ru*

***e-mail: tema@ikfia.ysn.ru*

Received February 22, 2019; revised March 22, 2019; accepted March 27, 2019

The lateral distribution of muons in extensive air showers with energies above 10^{17} eV detected by underground scintillation detectors with a threshold of ~1.0 GeV at the Yakutsk array in 1986–2016 has been analyzed. The experimental data on the muon flux density at a distance of 300 m from the shower axis have been compared to the calculations within various models of hadron interactions at ultrahigh energies. The experimental data are in the best agreement with the QGSJet01 and QGSJet II-04 models. The mass composition of cosmic rays in the energy range of $(1–30) \times 10^{17}$ eV changes from middle nuclei to a purely proton composition.

DOI: 10.1134/S0021364019090091

1. INTRODUCTION

Cosmic rays with ultrahigh energies (above 10^{15} eV) have been studied worldwide for more than five decades [1]. To date, their mass composition is not known exactly, and this circumstance complicates understanding the character of nuclear interactions at these energies. To estimate the mass composition, various parameters of extensive air showers (EASs) sensitive to the mass composition of cosmic rays are used. The lateral distribution functions of electron, muon, and Cherenkov components of EASs are used at the Yakutsk EAS array (see, e.g., [2–7]). The key parameter for determining the mass composition of cosmic rays is the maximum development depth $x_{\max}$ of an EAS, which is related to the atomic number A of primary particles by the simple relation

$$\langle \ln A \rangle = \frac{x_{\max}^{p} - x_{\max}^{\exp}}{x_{\max}^{p} - x_{\max}^{\mathrm{Fe}}} \ln 56 \qquad (1)$$

following from the nucleon superposition principle [8]. Here, $x_{\max}^{\exp}$ values are obtained experimentally, whereas $x_{\max}^{p}$ and $x_{\max}^{\mathrm{Fe}}$ values are calculated for primary protons and iron nuclei, respectively. Here, theoretical concepts of the development of EASs are necessary. In [9], the lateral distribution functions of signals from ground-based and underground scintillation detectors of the Yakutsk EAS array initiated by cosmic rays with energies $E_0 \geq 10^{17}$ eV were calculated. The lateral distribution functions of shower particles were obtained within the QGSJet01 [10], QGSJet II-04 [11], EPOS-LHC [12], and SIBYLL-2.1 [13] models in the CORSIKA package [14].

2. RESULTS

The fraction of muons determined at a distance of 300 m from the axis of EAS is the most sensitive parameter to the mass composition of cosmic rays. This parameter is reliably determined from the lateral distribution functions measured at the Yakutsk EAS array at energies $E_0 \geq 10^{17}$ eV as $\rho_\mu(300)/\rho_s(300)$, where $\rho_\mu(300)$ and $\rho_s(300)$ are the densities of muons and EAS particles measured at the distance $r = 300$ m from the axis by underground and ground-based scintillator detectors, respectively.

In this work, we analyze signals from three muon detectors each with the threshold $\epsilon_{\mathrm{thr}} \geq 1$ GeV and an area of 20 m^2 located at distances of 0.5–1.0 km from the center of the array. These detectors demonstrate the most stable operation during the entire time interval under consideration.

The densities of particles used to calculate the muon content in EASs were determined from the average lateral distribution functions of showers with zenith angles $\theta \leq 38.7^\circ$ ($\langle \cos\theta \rangle = 0.9$). The method

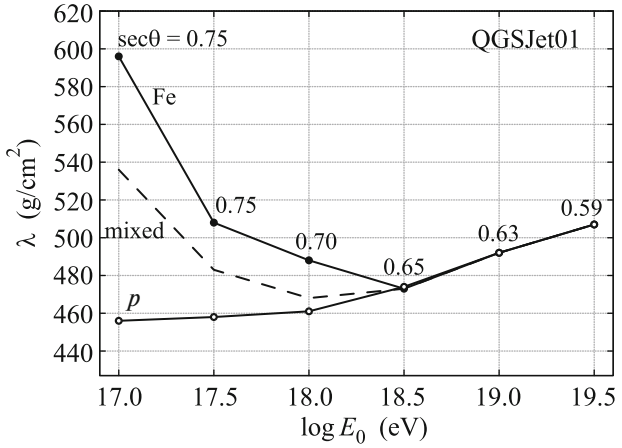

Fig. 1. Energy dependence of the absorption mean free path in Eq. (3) at the recalculation of the measured density of particles from inclined to vertical showers. The results for primary protons, mixed composition, and iron nuclei are obtained within the QGSJet01 model. Secants of maximum permissible zenith angles are given near the points.

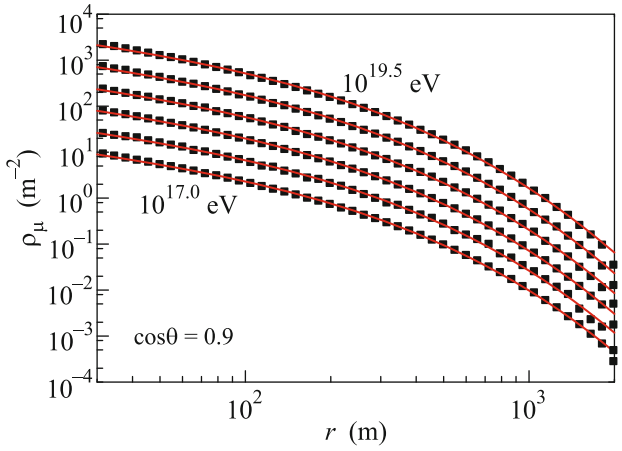

Fig. 2. (Color online) Lateral distribution function of muons with a threshold of ~1 GeV in showers with energies of 10^{17}–$10^{19.5}$ eV initiated by primary protons as calculated within the QGSJet01 model. Lines are analytical approximations by Eq. (6).

for constructing the lateral distribution functions to obtain $\rho_s(300)$ was described in [15]. The energy of primary particles was determined as

$$E_0 = (3.76 \pm 0.3) \times 10^{17} \rho_s(600, 0^\circ)^{1.02 \pm 0.02}, \quad (2)$$

where

$$\rho_s(600, 0^\circ) = \rho_s(600, \theta) \exp\left(\frac{1020(\sec\theta - 1)}{\lambda}\right). \quad (3)$$

Here, λ is the absorption mean free path in Fig. 1 [16] and $\rho_s(600, \theta)$ is the density of EAS particles with the zenith angle θ measured by ground-based detectors at a distance of 600 m from the axis.

The average lateral distribution functions of muons were constructed similarly [15] in energy ranges with the width $h = \Delta \log E_0 = 0.2$, which are successively shifted by $0.5h$ for a more detailed analysis of the agreement of the experiment with various models. The quantities $\rho_\mu(300)$ were obtained from the approximations of the average lateral distribution functions. When constructing the lateral distribution functions, the muon densities in individual showers were multiplied by the normalization coefficient $\langle E_0 \rangle / E_0$ and were averaged in the ranges of the distance from the axis with the width determined by the relation $\Delta \log r = 0.04$. The average muon densities were determined by the formula

$$\langle \rho_\mu(r_i) \rangle = \sum_{n=1}^{N_1} \frac{\rho_n(r_i)}{N_1 + N_0}, \quad (4)$$

where N_1 and N_0 are the numbers of nonzero and zero signals from muon detectors in the ranges $(\log r_i, \log r_i + 0.04)$ of the distance from the axis, respectively. Zero signals refer to the cases where detectors did not detect any muon but were in the waiting mode. The average lateral distribution functions of muons were approximated by the function

$$\rho_\mu(r, \theta) = f_\mu(r, \theta) \left(\frac{2000 + 600}{2000 + r}\right)^{6.5}. \quad (5)$$

Here,

$$f_\mu(r, \theta) = \rho_\mu(600, \theta) \left(\frac{600}{r}\right)^{0.75} \times \left(\frac{r_0 + 600}{r_0 + r}\right)^{b_\mu - 0.75} \quad (6)$$

is the Greisen function [17] with $r_0 = 280$ m and the free parameter b_μ. The b_μ and $\rho_\mu(600, \theta)$ values in Eq. (6) in each average lateral distribution function were determined in the process of χ^2 minimization. The desired $\rho_\mu(300, \theta)$ values were found from the resulting approximations. Figure 2 shows (points) the lateral distribution functions of muons with a threshold of 1.0 GeV obtained within the QGSJet01 model for primary protons in the energy range of 10^{17}–$10^{19.5}$ eV and $\cos\theta = 0.9$ and (lines) approximations by Eq. (6) obtained through χ^2 minimization.

The procedure of construction of the lateral distribution functions based on simulation data was described in detail in [9, 16]. Briefly, the reconstruction of $\rho_\mu(300)$ in the experiment and in calculations was performed identically from average experimental and calculated lateral distribution functions with fluctuations really present in both cases.

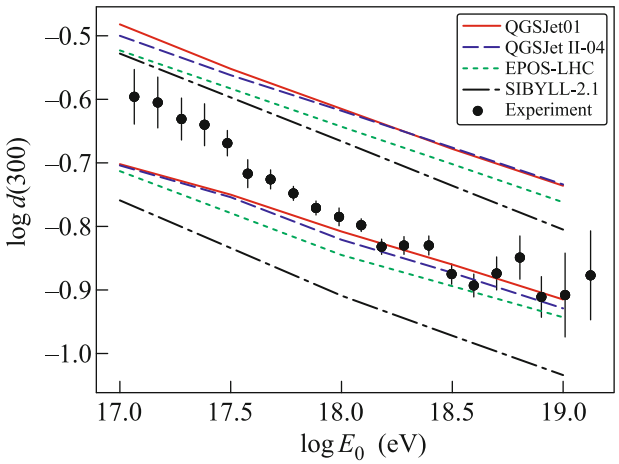

Fig. 3. (Color online) Energy dependence of the fraction of muons $d(300)$ with a threshold of ~1.0 GeV at a distance of 300 m from the axis in showers with $\langle\cos\theta\rangle = 0.90$ as calculated within several models of hadron interactions.

Points in Fig. 3 are the experimental data for the ratio $d = \rho_\mu(300)/\rho_s(300)$ in the above sample of showers. Error bars include total errors corresponding to the sampling of showers and the method of their averaging at the construction of the lateral distribution functions of both components of EASs. Lines are the calculations within various models of hadron interactions at ultrahigh energies for primary protons and iron nuclei. Table 1 presents values of the scaling factor z corresponding to this figure, which was introduced in [18] as

$$z = \frac{\ln d_{\rm exp} - \ln d_p}{\ln d_{\rm Fe} - \ln d_p}. \quad (7)$$

Here, $d_{\rm exp}$ is the experimental d value and d_p and $d_{\rm Fe}$ are the d values calculated for primary protons and iron nuclei within various models of hadron interactions, respectively. The scaling factor given by Eq. (7) is related to Eq. (1) by the formula

$$\ln A = z \ln 56 \quad (8)$$

convenient for estimating the mass composition of cosmic rays. Figure 4 shows the dependences of the mass composition of cosmic rays on the primary energy according to different EAS array data. Closed circles are our estimates of $\langle\ln A\rangle$ obtained from Eqs. (7) and (8) for the models presented in Fig. 3. Open circles are our estimates of the mass composition of cosmic rays from the shape of the lateral distri-

Table 1. Scaling parameter z calculated by Eq. (7) from the muon flux densities at a distance of 300 m from the axis of the EAS (see Fig. 3), the energy of primary particles E_0 estimated by Eq. (2), errors (err) including both systematic and statistical uncertainties, and the number of showers $N_{\rm sh}$ in the interval with a given average energy

E_0, eV ($\times 10^{17}$)	QGSJet01		QGSJet II-04		EPOS-LHC		SIBYLL-2.1		$N_{\rm sh}$
	z	err	z	err	z	err	z	err	
1.016	0.528	0.200	0.571	0.200	0.652	0.200	0.732	0.200	5172
1.480	0.534	0.180	0.562	0.180	0.670	0.180	0.770	0.180	5644
1.910	0.460	0.160	0.521	0.160	0.632	0.160	0.719	0.160	6079
2.410	0.560	0.165	0.589	0.165	0.708	0.165	0.824	0.165	6137
3.050	0.392	0.130	0.426	0.130	0.546	0.130	0.672	0.130	6182
3.780	0.206	0.105	0.234	0.105	0.364	0.105	0.544	0.105	5685
4.770	0.208	0.100	0.253	0.100	0.385	0.100	0.560	0.100	4807
6.070	0.170	0.060	0.208	0.060	0.333	0.060	0.534	0.060	3778
7.670	0.108	0.060	0.198	0.060	0.296	0.060	0.517	0.060	2717
9.710	0.106	0.082	0.149	0.082	0.286	0.082	0.508	0.082	1881
12.30	0.100	0.060	0.140	0.060	0.276	0.060	0.517	0.060	1316
15.20	–0.044	0.065	0.046	0.065	0.167	0.065	0.431	0.065	934
19.10	0.046	0.075	0.118	0.075	0.219	0.075	0.483	0.075	600
24.20	0.088	0.088	0.190	0.088	0.276	0.088	0.552	0.088	403
31.30	–0.090	0.108	0.000	0.108	0.106	0.108	0.421	0.108	260
40.60	–0.115	0.105	–0.048	0.105	0.065	0.105	0.478	0.105	150
51.20	0.045	0.155	0.132	0.155	0.206	0.155	0.526	0.155	107
63.10	0.250	0.180	0.341	0.180	0.400	0.180	0.702	0.180	87
81.60	–0.044	0.182	0.048	0.182	0.122	0.182	0.482	0.182	60
103.0	0.045	0.362	0.134	0.362	0.204	0.362	0.562	0.362	29
136.0	0.290	0.375	0.402	0.375	0.432	0.375	0.759	0.375	16

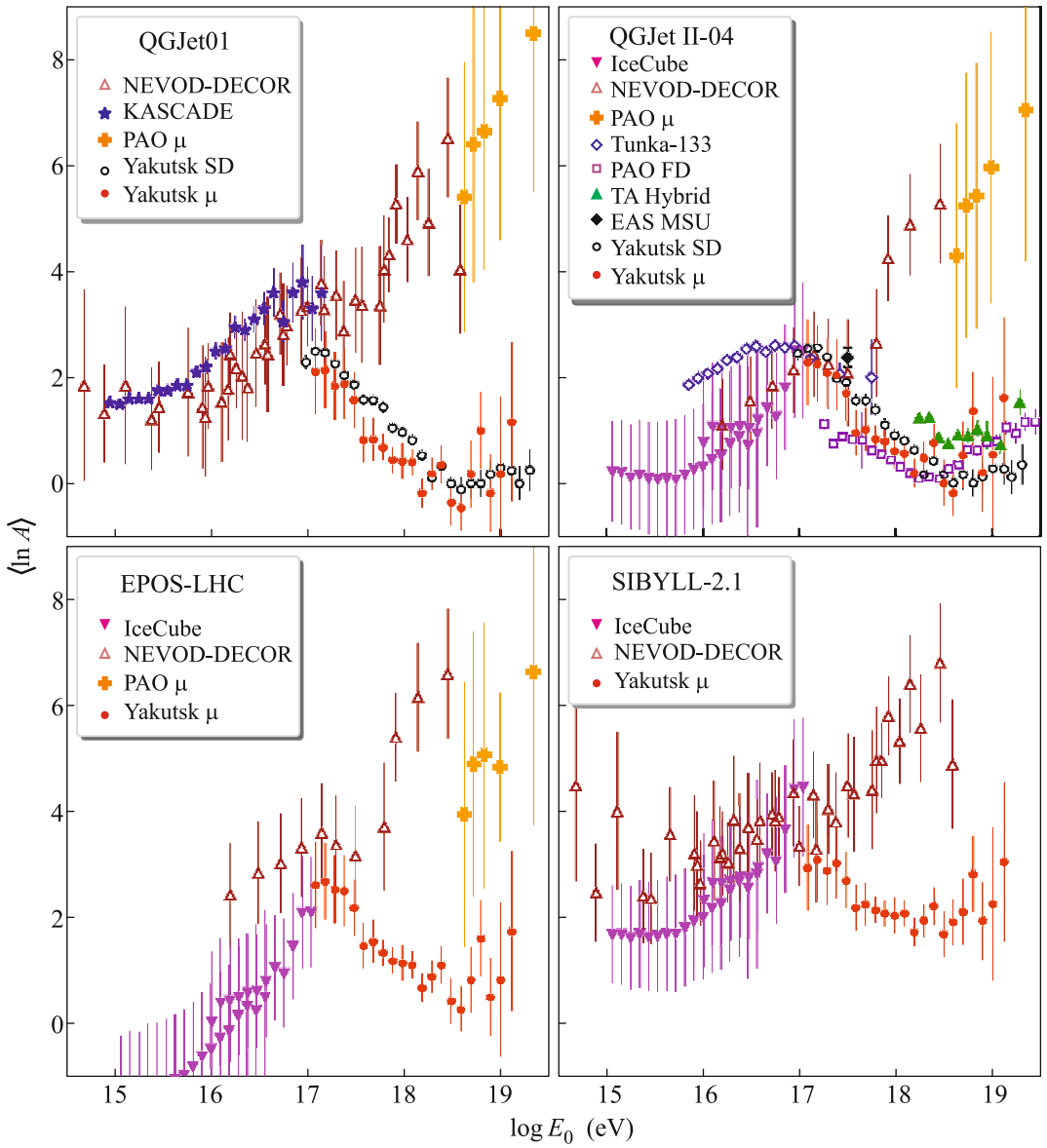

Fig. 4. (Color online) Energy dependences of the mass composition of cosmic rays obtained at different EAS arrays. Open circles (Yakutsk SD) are estimates obtained from data from the ground-based detectors of the Yakutsk EAS array [15] and closed circles (Yakutsk μ) are estimates obtained from the muon component of EASs. Also shown are estimates obtained from the scaling parameter z [18] for IceCube [19], NEVOD-DECOR [20, 21], PAO [23–25], and EAS-MGU [22] experiments, as well as data from the KASCADE array [26], Tunka-133 array [27], fluorescent part of the PAO (PAO FD) [28], and TA array [29, 30].

bution function measured by ground-based scintillation detectors [15]. The other symbols are estimates of $\langle \ln A \rangle$ obtained from Eq. (8) using the scaling factor z [18] for IceCube [19], NEVOD-DECOR [20, 21], EAS-MGU [22], and Pierre Auger Observatory (PAO) [23–25] experiments, where the muon component of EASs was measured. Also shown are the KASCADE array data collected from May 1998 to December 1999 [26], Tunka-133 array data obtained from the lateral distribution function of Cherenkov radiation of EASs [27], estimates according to data from fluorescent detectors of the PAO [28], and Telescope Array (TA) data [29, 30].

3. CONCLUSIONS

Long-term measurements of the muon component of extensive air showers with the threshold $\epsilon_{thr} \simeq 1.0$ GeV at the Yakutsk EAS array have made it possible to estimate the mass composition of cosmic rays in the energy range $E_0 \approx 10^{17}$–$10^{19.5}$ eV, where the experimental data are still scarce. Figure 4 demonstrates that, according to the QGSJet01 and QGSJet II-04

models, the mass composition of cosmic rays changes rapidly with an increase in the energy in the range of $(1-30) \times 10^{17}$ eV toward lighter nuclei. This is probably due to the transition from Galactic cosmic rays to extragalactic cosmic rays. According to our data and TA estimates [29, 30], it can be assumed that protons are predominant primary particles at energies $E_0 \geq 3\times10^{18}$ eV. However, such a conclusion cannot yet be made strictly. The PAO data [28] indicate that the mass of primary nuclei increases with the energy. These data below $\sim 3 \times 10^{17}$ eV contradict our estimates and estimates obtained at the KASCADE [26] and Tunka-133 [27] arrays. A significant difference of the NEVOD-DECOR [20, 21] and PAO [23–25] experimental results from the results mentioned above is apparently due to features of methods used in those experiments. Further investigations are required and we are planning them.

REFERENCES

1. P. K. F. Grieder, *Extensive Air Showers: High Energy Phenomena and Astrophysical Aspects* (Springer, Berlin, 2010).
2. A. V. Glushkov, V. M. Grigoriev, N. N. Efimov, M. I. Pravdin, O. S. Diminstein, and V. P. Sokurov, in *Proceedings of the 16th ICRC, Kyoto, 1979,* Ed. by S. Miyake and N. Gakujutsu Kaigi (Tokyo, 1979), p. 158.
3. A. V. Glushkov, Cand. Sci. Dissertation (Skobeltsyn Inst. Nucl. Phys., Moscow State Univ., Moscow, 1982).
4. A. V. Glushkov, L. G. Dedenko, N. N. Efimov, N. N. Efremov, I. T. Makarov, P. D. Petrov, and M. I. Pravdin, Izv. Akad. Nauk SSSR, Ser. Fiz. **55**, 2166 (1986).
5. A. V. Glushkov, M. I. Pravdin, I. E. Sleptsov, V. R. Sleptsova, and N. N. Kalmykov, Phys. At. Nucl. **63**, 1477 (2000).
6. A. V. Glushkov and A. V. Saburov, JETP Lett. **98**, 589 (2013).
7. E. G. Berezhko, S. P. Knurenko, and L. T. Ksenofontov, Astropart. Phys. **36**, 31 (2013).
8. J. R. Hörandel, J. Phys.: Conf. Ser. **47**, 41 (2006).
9. A. V. Saburov, Cand. Sci. Dissertation (Inst. Nucl. Res. RAS, Moscow, 2018).
10. N. N. Kalmykov, S. S. Ostapchenko, and A. I. Pavlov, Nucl. Phys. B Proc. Suppl. **52**, 17 (1997).
11. S. Ostapchenko, Phys. Rev. D **83**, 014018 (2011); arXiv:1010.1869 [hep-ph].
12. T. Pierog, Iu. Karpenko, J. M. Katzy, E. Yatsenko, and K. Werner, Phys. Rev. C **92**, 034906 (2015); arXiv:1306.0121 [hep-ph].
13. E.-J. Ahn, R. Engel, T. K. Gaisser, P. Lipari, and T. Stanev, Phys. Rev. D **80**, 094003 (2009); arXiv:0906.4113 [hep-ph].
14. D. Heck, J. Knapp, J. N. Capdevielle, G. Schatz, and T. Thouw, Forschungszentrum Karlsruhe Report FZKA 6019 (Karlsruhe, 1988).
15. A. V. Glushkov, M. I. Pravdin, and A. V. Saburov, Astron. Lett. **44**, 588 (2018).
16. A. V. Glushkov, M. I. Pravdin, and A. V. Saburov, Phys. At. Nucl. **81**, 575 (2018).
17. K. Greisen, Annu. Rev. Nucl. Sci. **10**, 63 (1960).
18. H. P. Dembinsky, J. C. Arteaga-Velázquez, L. Cazon, et al. (for the WHISP group), in *Proceedings of the UHECR2018, Paris, 2018,* Talk ID 64367, EPJ Web of Conf. (2019, in press); arXiv: 1902.08124 [astro-ph.HE].
19. J. G. Gonzales, M. G. Aartsen, M. Ackermann, et al. (IceCube Collab.), in *Proceedings of the 20th ISVHECRI, Nagoya, 2018,* Talk ID 2964861, EPJ Web of Conf. (2019, in press).
20. A. G. Bogdanov, D. M. Gromushkin, R. P. Kokoulin, G. Mannocchi, A. A. Petrukhin, O. Saavedra, G. Trinchero, D. V. Chernov, V. V. Shutenko, and I. I. Yashin, Phys. At. Nucl. **73**, 1852 (2010).
21. A. G. Bogdanov, R. P. Kokoulin, G. Mannocchi, A. A. Petrukhin, O. Saavedra, V. V. Shutenko, G. Trinchero, and I. I. Yashin, Astropart. Phys. **98**, 13 (2018).
22. Yu. A. Fomin, N. N. Kalmykov, I. S. Karpikov, G. V. Kulikov, M. Yu. Kuznetsov, G. I. Rubtsov, V. P. Sulakov, and S. V. Troitsky, Astropart. Phys. **92**, 1 (2017); arXiv:1609.05764 [astro-ph.HE].
23. A. Aab, P. Abreu, M. Aglietta., et al. (Pierre Auger Collab.), Phys. Rev. D **91**, 032003 (2015); arXiv:1408.1421 [astro-ph.HE].
24. A. Aab, P. Abreu, M. Aglietta, et al. (Pierre Auger Collab.), Phys. Rev. Lett. **117**, 192001 (2016); arXiv:1610.08509 [hep-ex].
25. S. Müller, A. Aab, P. Abreu, et al. (Pierre Auger Collab.), in *Proceedings of the UHECR2018, Paris, 2018,* Talk ID 65721; EPJ Web of Conf. (2019, in press).
26. H. Ulrich, T. Antoni, W. D. Apel, et al. (KASCADE Collab.), in *Proceedings of the 27th ICRC, Hamburg, 2001,* Ed. by K.-H. Kampert, G. Hainzelmann, and C. Spiering (Copernicus, Berlin, 2001), Vol. 2, p. 97.
27. V. V. Prosin, S. F. Berezhnev, N. M. Budnev, et al. (Tunka Collab.), Nucl. Instrum. Methods Phys. Res., Sect. A **756**, 94 (2014).
28. J. Bellido (for the Pierre Auger Collab.), in *Proceedings of the 35th ICRS, Busan, 2017,* PoS(ICRC2017)506.
29. R. U. Abbasi, M. Abe, T. Abu-Zayyad, et al. (Telescope Array Collab.), Astrophys. J. **858**, 76 (2018); arXiv:1801.09784 [astro-ph.HE].
30. R. U. Abbasi, M. Abe, T. Abu-Zayyad, et al. (Telescope Array Collab.), Phys. Rev. D **99**, 022002 (2019); arXiv:1808.03680 [astro-ph.HE].

Translated by R. Tyapaev